International Journal of Heat and Mass Transfer 52 (2009) 3091–3100

Contents lists available at ScienceDirect

International Journal of Heat and Mass Transfer

journal homepage: www.elsevier.com/locate/ijhmt

Ultrafast solid–liquid–vapor phase change in a thin gold film irradiated by multiple femtosecond laser pulses

Jing Huang, Yuwen Zhang *, J.K. Chen

Department of Mechanical and Aerospace Engineering, University of Missouri, Columbia, MO 65211, USA

ARTICLE INFO

Article history:
Received 5 January 2009
Received in revised form 9 February 2009
Accepted 9 February 2009
Available online 26 March 2009

Keywords:
Femtosecond laser
Melting, vaporization
Metal film
Interface tracking

ABSTRACT

Phase change processes including melting, vaporization and resolidification during the multiple femtosecond laser pulses irradiations on a thin gold film are investigated numerically. A two-temperature model is coupled with the phase interface track methods to describe the temperature variation and the solid–liquid and liquid–vapor interface evolutions. The relationship between the maximum vaporization temperature and melting depth, ablation depth are analyzed and compared with that of the single pulse irradiation. It is found that for two pulses irradiation, if deeper melting depth is desirable, the second pulse should be launched as soon as the melting depth induced by the first pulse reaches to the maximum. In comparison to a single pulse irradiation resulting in the same lattice temperature, this two-pulse approach leads to a greater melting depth. For laser irradiation with more than two consecutive pulses, if the total laser fluence remains a constant, larger pulse number and longer separation times between pulses leads to a smaller melting depth. However, the melting depth is much deeper compared to that by induced by a single pulse that causes the same lattice temperature.

© 2009 Elsevier Ltd. All rights reserved.

1. Introduction

Phase changes are widely encountered in laser-material processing, such as laser cutting, cladding, welding, surface treatment, and Selective Laser Sintering (SLS). In SLS with a short-pulse laser, for example, it is often desired that the interaction of the laser beam with the powder particles raises the surface temperature to the melting point and causes partial melting of the particle. Resolidification of the liquid layer at the particle surface causes powder particles to bind together. The porosity of the part fabricated by SLS can be controlled by controlling the maximum melting depth through adjustment of the laser processing parameters. In pulsed laser machining, a focused beam heats up the workpiece to its boiling point and the material is removed by vaporization.

Numerous research works have been carried out to study phase change processes, including melting, evaporation and resolidification induced by laser pulse irradiation, using different methods and aiming at different applications [1–7]. While CW lasers were exclusively studied by the early researchers, pulsed laser has drawn much more attentions recently due to its high efficiency, high power density and many other unique merits. When the duration of a laser pulse is around or less than 10^{-13} s, which is the mean free time between collisions of electrons in metals, nonequilibrium between electrons and the lattice becomes significant and cannot be analyzed by the classical heat transfer models. Two-temperature model, which was originally put forward by Anisimov et al. [8] and then rigorously derived by Qiu and Tien [9] based on the Boltzmann equation, is widely accepted for simulating femtosecond laser-material interactions. The dual-phase-lag model by considering lagging behavior of different energy carriers [10,11] is identical to the two-temperature model if material thermophysical properties are constant. Jiang and Tsai extended the existing two-temperature model to high electron temperatures with full-run quantum treatments [12]. Chen et al. [13] proposed a semiclassical two-step heating model to investigate thermal transport in metals caused by ultrashort laser irradiation. While the above works consider pure conduction only, the authors developed a model that can track the evolution of both solid–liquid and liquid–vapor interfaces in a thin metal film under single ultrashort laser pulse interaction [14].

One of the key issues in laser-material processing is to control residual thermal stress. Rapid cooling of the melted part will cause thermal distortion due to uncontrolled temperature distribution. Generally, lower peak temperature and smaller temperature gradient are helpful to reduce the undesirable residual stress. For single pulse irradiation, the only controllable parameters are the fluence and temporal shape of the laser beam. To obtain better control of the phase change processes and reduce the peak temperature, multiple consecutive pulses can be employed. The experiment conducted by Chowdhurry et al. [15] proved that by splitting a single pulse into four pulses at separations ranging from 1 ps to

* Corresponding author.
E-mail address: zhangyu@missouri.edu (Y. Zhang).

0017-9310/$ - see front matter © 2009 Elsevier Ltd. All rights reserved.
doi:10.1016/j.ijheatmasstransfer.2009.02.009

Nomenclature

Be	coefficient for electron heat capacity (J/m^3 K^2)
C	heat capacity (J/m^3 K)
c_p	specific heat (J/kg K)
G	electron–lattice coupling coefficient (W/m^3 K)
h	latent heat of phase change (J/kg)
J	heat source fluence (J/m^2)
k	thermal conductivity (W/m K)
L	thickness of the metal film (m)
M	molar mass (kg/kmol)
p	pressure (Pa)
q''	heat flux (W/m^2)
R	reflectivity
R_g	specific gas constant (J/kg K)
R_u	universal gas constant (J/kmol K)
s	interfacial location (m)
S	intensity of the internal heat source (W/m^3)
t	time (s)
t_p	pulse width (s)
T	temperature (K)
T_F	Fermi temperature (K)
T_m	melting point (K)
u	interfacial velocity (m/s)
V_0	interfacial velocity factor (m/s)
x	coordinate (m)

Greek symbols

δ	optical penetration depth (m)
δ_b	ballistic range (m)
ε	total emissivity
ρ	density (kg/m^3)
σ	Stefan–Boltzmann constant (W/m^2 K^4)

Superscript

0	last time step

Subscripts

0	initial condition
e	electron
eq	thermal equilibrium state
i	pulse sequence
l	lattice
ℓ	liquid
ℓv	liquid–vapor interface
R	thermal radiation
s	solid
$s\ell$	solid–liquid interface
sur	surface
∞	ambient environment

1 ns, a better material removal rate can be achieved. Chen and Beraun [16] set up a model to study the material ablation caused by phase explosion and found that if the first pulse fluence is higher than the ablation threshold, two consecutive pulses split from a single laser pulse could ablate more material. The best time for the second pulse to impinge is right after the material ablation by the first pulse is completed. Jiang and Tsai [17] studied the ultrashort laser pulse-train processing of gold thin films. Their simulation results show that using multiple consecutive pulses would increase the photon efficiency, and less total laser energy is required to achieve the same lattice temperature than a single pulse.

In this paper, based on a numerical model which can describe the ultrafast melting and evaporation processes, the rapid solid–liquid–vapor phase change in a free standing gold film induced by irradiation of multiple femtosecond laser pulses will be studied numerically. The effects of laser fluence and separation time between pulses on melting depth, ablation depth and peak temperature will be discussed in detail.

2. Physical model

Fig. 1 shows the physical model of the problem under consideration. Each laser pulse impinging on the right side of a free standing gold film is assumed to be temporally Gaussian. The pulse duration (t_p), defined as the full width at half maximum (FWHM), is fixed to be 100 fs in the current work. The separation time Δt is defined as the interval between the peaks of two consecutive pulses. The gold film has a thickness of L, which is very small in comparison to the radius of the laser beam; therefore this problem can be approximated to be one-dimensional.

The two-step heating model for free electrons and the lattice are [8]

$$C_e\frac{\partial T_e}{\partial t}=\frac{\partial}{\partial x}\left(k_e\frac{\partial T_e}{dx}\right)-G(T_e-T_l)+S \tag{1}$$

$$C_l\frac{\partial T_l}{\partial t}=\frac{\partial}{\partial x}\left(k_l\frac{\partial T_l}{dx}\right)+G(T_e-T_l) \tag{2}$$

The heat capacity of electrons C_e, as suggest by Chen et al. [13], is approximated by

$$C_e=\begin{cases}B_eT_e, & T_e<T_F/\pi^2\\ 2B_eT_e/3+C'_e/3, & T_F/\pi^2\leqslant T_e<3T_F/\pi^2\\ Nk_B+C'_e/3, & 3T_F/\pi^2\leqslant T_e<T_F\\ 3Nk_B/2, & T_e\geqslant T_F\end{cases} \tag{3}$$

where

$$C'_e=B_eT_F/\pi^2+\frac{3Nk_B/2-B_eT_F/\pi^2}{T_F-T_F/\pi^2}(T_e-T_F/\pi^2) \tag{4}$$

The thermal conductivity of electron k_e can be obtained by [18]

$$k_e=\chi\frac{(\vartheta_e^2+0.16)^{5/4}(\vartheta_e^2+0.44)\vartheta_e}{(\vartheta_e^2+0.092)^{1/2}(\vartheta_e^2+\eta\vartheta_l)} \tag{5}$$

where $\vartheta_e=T_e/T_F$ and $\vartheta_l=T_l/T_F$.

In Eqs. (1) and (2), G is the electron–lattice coupling factor. A phenomenological temperature-dependent G suggested by Chen et al. [19] is adopted:

$$G=G_{RT}\left[\frac{A_e}{B_1}(T_e+T_l)+1\right] \tag{6}$$

Since the electrons are more likely to collide with liquid atoms than the atoms in solid crystals, in the liquid phase, G, is taken to be 20% higher than that of the solid [20].

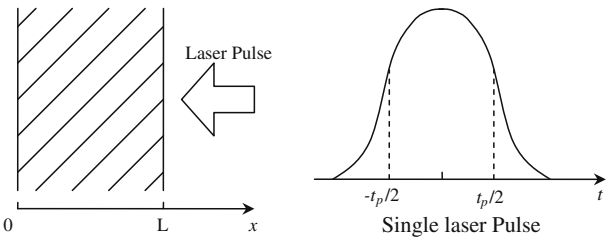

Fig. 1. Laser irradiation on thin film.

The laser irradiation is considered as a source term S in Eq. (1):

$$S = \sum_{i=1}^{N} 0.94 J_i \frac{1-R}{t_p(\delta+\delta_b)[1-e^{-L/(\delta+\delta_b)}]} \times \exp\left[-\frac{x}{(\delta+\delta_b)} - 2.77\left(\frac{t-t_i}{t_p}\right)^2\right] \quad (7)$$

where N is the number of pulses in a burst, t_i is the time when the corresponding single pulse reaches its peak, R is the reflectivity of the thin film, δ is the optical penetration depth, J is the laser pulse fluence, δ_b is the ballistic depth, and $[1-e^{-L/(\delta+\delta_b)}]$ is to correct the film thickness effect.

For a metal at equilibrium, the thermal conductivity, k_{eq}, is the sum of the electron thermal conductivity, k_e, and the lattice thermal conductivity, k_l. In most cases k_e dominates k_{eq} because free electrons contribute to the majority part of heat conduction, For gold, k_l is usually taken to be 1% of k_{eq} [21], i.e.,

$$k_l = 0.01 k_{eq} \quad (8)$$

A uniform temperature distribution is set to be the initial condition:

$$T_e(x,-2t_p) = T_l(x,-2t_p) = T_0 \quad (9)$$

On the right side of the film which receives laser irradiation, the heat loss caused by radiation will be considered while on the other side adiabatic boundary condition is applied:

$$\left.\frac{\partial T_e}{\partial x}\right|_{x=0} = \left.\frac{\partial T_e}{\partial x}\right|_{x=L} = \left.\frac{\partial T_l}{\partial x}\right|_{x=0} = 0 \quad (10)$$

$$q''_R|_{x=L} = \sigma\varepsilon(T_{sur}^4 - T_\infty^4) \quad (11)$$

Before onset of evaporation, T_{sur} is the surface lattice temperature at $x = L$. Once evaporation begins, T_{sur} is the liquid–vapor interface temperature which varies with the heating condition and needs to be determined.

The energy balance at the solid–liquid interface is described by [22]:

$$k_{l,s}\frac{\partial T_{l,s}}{\partial x} - k_{l,\ell}\frac{\partial T_{l,\ell}}{\partial x} = \rho_\ell h_m u_{s\ell} \qquad x = s(t) \quad (12)$$

where $T_{l,s}$ and $T_{l,\ell}$ are, respectively, solid and liquid lattice temperature, ρ is the density, h_m is latent heat of fusion, and u_s is solid–liquid interfacial velocity. The additional interfacial velocity due to the density change during melting and resolidification has been considered.

For rapid melting/solidification processes, the velocity of the interface is dominated by nucleation dynamics, instead by energy balance, Eq. (12). For ultrashort-pulsed laser melting of gold, the velocity of the solid–liquid interface is described by [20]

$$u_{s\ell} = V_0\left[1 - \exp\left(-\frac{h_m}{R_g T_m}\frac{T_{l,I}-T_m}{T_{l,I}}\right)\right] \quad (13)$$

where V_0 is the maximum interface velocity, R_g is the gas constant for the metal, and $T_{l,I}$ is the interfacial temperature. The interfacial temperature, $T_{l,I}$, is higher than the normal melting point, T_m, during melting and lower than T_m during solidification.

For the liquid–vapor interface, energy balance at the interface and the vaporization rules derived from kinetics laws will be applied to find its temperature, velocity, and location. The energy balance at the liquid–vapor interface is:

$$\rho h_{\ell v} u_{\ell v} + \sigma\varepsilon(T_{\ell v}^4 - T_\infty^4) = -k_l\frac{\partial T_l}{\partial x} \quad (14)$$

where $h_{\ell v}$ is the latent heat of evaporation of gold, $u_{\ell v}$ is the velocity of the interface, $T_{\ell v}$ is the temperature of the interface. With a known interface velocity, Eq. (14) will be used to calculate the interface temperature $T_{\ell v}$.

To characterize the vaporization process, Clausius–Clapeyron equation is employed to describe the slope of saturation pressure–temperature curve, with the assumption of ideal gas and thermal equilibrium:

$$\frac{dp}{dT_{\ell v}} = \frac{p h_{\ell v}(T_{\ell v})}{R_u T_{\ell v}^2} \quad (15)$$

where R_u is the universal gas constant, which is related to boiling temperature T *as:*

$$h_{\ell v}(T_{\ell v}) = h_{\ell v 0}\left[1 - \left(\frac{T_{\ell v}}{T_c}\right)^2\right]^{1/2} \quad (16)$$

where $h_{\ell v 0}$ is the latent heat of vaporization at absolute zero and T_c is the critical temperature [23]. By integrating Eq. (15), the relationship between interfacial temperature and pressure can be obtained as:

$$p = p_0 \exp\left\{-\frac{\rho_\ell L_0}{R_u}\left[\frac{1}{T_{\ell v}}\sqrt{1-\left(\frac{T_{\ell v}}{T_c}\right)^2} - \frac{1}{T_b}\sqrt{1-\left(\frac{T_b}{T_c}\right)^2}\right] - \frac{\rho_\ell L_0}{R_u T_c}\left[\sin^{-1}\left(\frac{T_{\ell v}}{T_c}\right) - \sin^{-1}\left(\frac{T_b}{T_c}\right)\right]\right\} \quad (17)$$

The molar evaporation flux j_v at the surface can be calculated by Hertz–Knudsen–Langmuir equation derived from kinetic theory of gases [24],

$$j_v = \frac{Ap}{\sqrt{2\pi M R_u T_{\ell v}}} \quad (18)$$

where A is an accommodation coefficient that shows which portion of vapor molecules striking the liquid–vapor surface is absorbed by this surface [25]. Xu et al. [23] recommended a value of 0.82 for this coefficient. The liquid–vapor interfacial velocity can be obtained from j_v as given below:

$$u_{\ell v} = \frac{M j_v}{\rho_\ell} = \frac{AMp}{\rho_\ell\sqrt{2\pi M R_u T_{\ell v}}} \quad (19)$$

It should be noted that while normal evaporation is the dominant mechanism for material ablation when the liquid temperature is below $0.9T_c$, phase explosion can take place when the liquid temperature reaches to $0.9T_c$. In this work, only the ablation caused by evaporation is considered, so the pulse fluence is controlled to avoid the lattice temperature to exceed $0.9T_c$.

3. Numerical solution

The computational domain is discretized using fixed uniform grid with 2052 control volumes. On each control volume, the discretized electron temperature equation is arranged as:

$$a_{e,P}T_{e,P} = a_{e,W}T_{e,W} + a_{e,E}T_{e,E} + a_{e,P}^0 T_{e,P}^0 + b_e \quad (20)$$

where:

$$a_{e,W} = \frac{k_{e,w}}{\delta x_w} \quad (21)$$

$$a_{e,E} = \frac{k_{e,e}}{\delta x_e} \quad (22)$$

$$a_{e,P}^0 = \frac{C_{e,P}\Delta x}{\Delta t} \quad (23)$$

$$b = G T_{l,P}^* \Delta x \quad (24)$$

$$a_{e,P} = a_{e,P}^0 + a_{e,W} + a_{e,E} + G\Delta x \quad (25)$$

Similarly, by integrating Eq. (2) on each control volume, the lattice energy equation can be obtained and rearranged as:

$$a_{l,P}T_{l,P} = a_{l,E}T_{l,E} + a_{l,W}T_{l,W} + a^0_{l,P}T^0_{l,P} + b_l \tag{26}$$

where:

$$a_{l,W} = \frac{k_{l,w}}{\delta x_w} \tag{27}$$

$$a_{l,E} = \frac{k_{l,e}}{\delta x_e} \tag{28}$$

$$a^0_{l,P} = \frac{C_{l,P}\Delta x}{\Delta t} \tag{29}$$

$$b = GT^*_{e,P}\Delta x \tag{30}$$

$$a_{l,P} = a^0_{l,P} + a_{l,W} + a_{l,E} + G\Delta x \tag{31}$$

In each time step, an iterative procedure is employed to deal with the non-linear relationship between electron energy equation, lattice energy equation, solid–liquid interface and liquid–vapor interface. Electron energy equation (20) will be solved first using tri-diagonal matrix method (TDMA), then the lattice energy equation (26) will be solved. After obtaining an estimated electron and lattice temperature field, the velocity and temperature of solid–liquid interface will be calculated by using the method provided in Ref. [26], which is repeated briefly here:

(1) The solid–liquid interfacial temperature T_{sl} is assumed and the solid–liquid phase interfacial velocity is determined according to the interfacial energy balance;
(2) The interfacial velocity from the nucleation dynamics is obtained from Eq. (13);
(3) The interfacial velocities got from Steps (1) and (2) are compared. If the interfacial velocity obtained from the energy balance is higher than that from the nucleation dynamics, the interfacial temperature will be increased; otherwise, the interfacial temperature is decreased.

Steps (1)–(3) are repeated until the difference between the interfacial velocities obtained from the two methods is less than 10^{-5} m/s.

The following iterative procedure will be employed to track the liquid–vapor interface:

(1) Assume an interfacial velocity $V^*_{\ell v}$, then the new interface location $s^*_{\ell v}$ is determined;
(2) Solve the energy balance equation at the liquid–vapor interface, Eq. (14), to obtain the interface temperature $T_{\ell v}$;
(3) According to Eqs. (17) and (19), obtain the new interface velocity $V^{**}_{\ell v}$;
(4) Go to Step 2 and use $V^{***}_{\ell v}$ as the new interface velocity.

Steps (2)–(4) are repeated until the difference between the interfacial velocities obtained from two consecutive iterations is less than 10^{-5} m/s. After obtaining the estimated locations of solid–liquid and liquid–vapor interfaces, the material properties in the electrons and lattice energy equations will be re-evaluated and Eqs. (26) and (20) will be solved again. The above procedures will be repeated till the maximum difference between the lattice temperatures obtained from two consecutive iterative steps is less than 10^{-5} K.

4. Results and discussion

The gold film thickness for all cases is fixed at 1 μm in the current work. The initial temperature T_0, is set to be 300 K. The laser pulse duration is 100 fs. The thermophysical and optical properties are given in Table 1.

4.1. Single pulse

To provide benchmark for the cases of multiple pulses, melting, evaporation and resolidification processes caused by single pulse irradiation are studied first. For a single pulse of 0.5 J/cm^2, the evolutions of surface electron and lattice temperature, the solid–liquid interface velocity and location, and the liquid–vapor interface velocity and location are shown in Fig. 2. It can be seen that electron temperature rapidly shoots up to 22,000 K due to their low heat capacity, and the lattice temperature reaches to its peak at 20 ps. Melting begins from the irradiated surface at t = 2.4 ps when the lattice temperature is 1336 K. Evaporation starts at about 12.7 ps and stops at about 43.5 ps. The melting process continues until a maximum melting depth of 143.5 nm is reached at 756 ps, then melting ceases and the liquid metal starts to resolidify.

In the current model, the melting and resolidification processes are controlled by nucleation dynamics. The solid–liquid interface can be heated well above the normal melting point (1336 K) and the solid can become superheated. Fig. 3(a) shows the dependence

Table 1
Thermophysical and optical properties of gold.

Coefficient for electronic heat capacity, B_e		70 [9]
Material constant, A_e		1.2×10^7 [19]
Material constant, B_1		1.23×10^{11} [19]
Electron–lattice coupling factor at room temperature, G_{RT} (W/m^3 K)	Solid	2.2×10^{16} [19]
	Liquid	2.6×10^{16} [19]
Specific heat, C_p (J/kg K)	Solid	$105.1 + 0.2941T_1 - 8.731 \times 10^{-4}T_1^2 + 1.787 \times 10^{-6}T_1^3 - 7.051 \times 10^{-10}T_1^4 + 1.538 \times 10^{-13}T_1^5$ [15]
	Liquid	163.205 [20]
Latent heat of evaporation at T_b, h_{lv} (J/kg)		1.698×10^6 [27]
Latent heat of fusion, h_m (J/kg)		6.373×10^4 [27]
Molar weight, M (kg/kmol)		196.967 [27]
Reflection coefficient, R		0.6
Universal gas constant, R_u (J/K kmol)		8314.0
Boiling temperature, T_b (K)		3127
Critical temperature, T_c (K)		5590
Melting temperature, T_m (K)		1336
Fermi temperature, T_F (K)		6.42×10^4
Limit velocity, V_0 (m/s)		1300 [20]
Coefficient for electronic conductivity, χ (W/m K)		353 [18]
Optical penetration depth, δ (nm)		20.6
Ballistic range, δ_b (nm)		105 [20]
Thermal conductivity at equilibrium, k_{eq} (W/m K)	Solid	$320.973 - 0.0111T_1 - 2.747 \times 10^{-5}T_1^2 - 4.048 \times 10^{-9}T_1^3$
	Liquid	$37.72 + 0.0711T_1 - 1.721 \times 10^{-5}T_1^2 + 1.064 \times 10^{-9}T_1^3$
Density, ρ (kg/m^3)	Solid	19.3×10^3
	Liquid	17.28×10^3

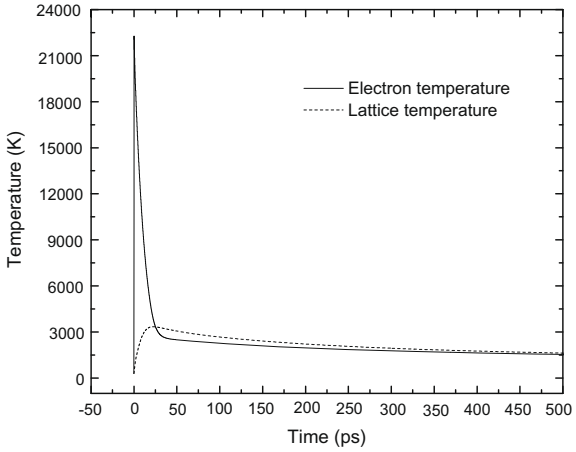

(a) Electron and lattice temperature

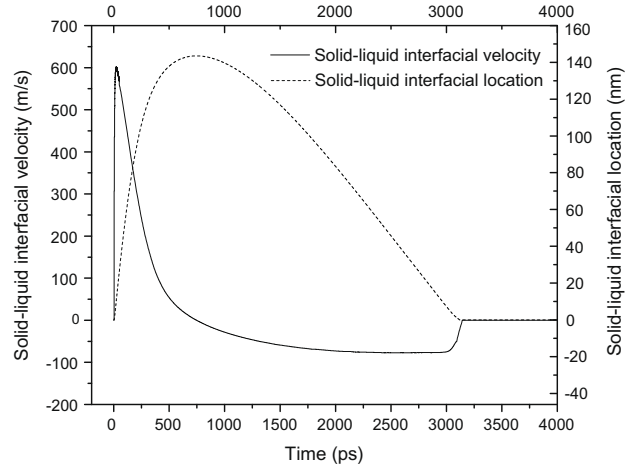

(b) Solid-liquid interfacial velocity and location

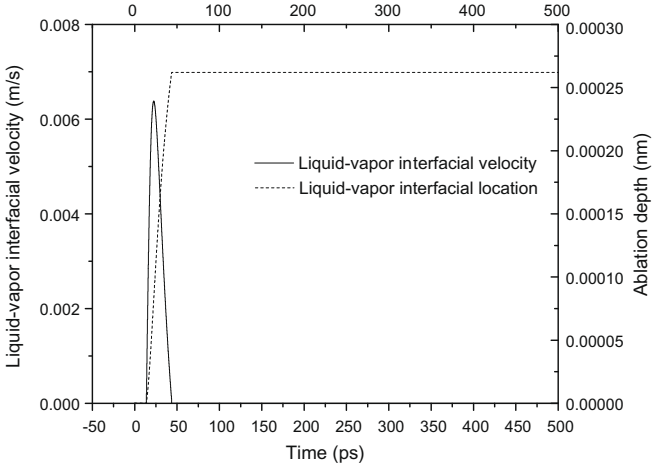

(c) Liquid-vapor interfacial velocity and location

Fig. 2. Irradiation by a 0.5 J/cm^2 single laser pulse.

of maximum solid–liquid interfacial temperature on laser fluence. It can be seen that in all cases superheating take place during the melting process and higher laser fluence leads to higher degree of superheating. Fig. 3(b) shows the relationship between the maximum lattice temperature and maximum melting depth. Obviously, higher pulse fluence leads to a deeper melting.

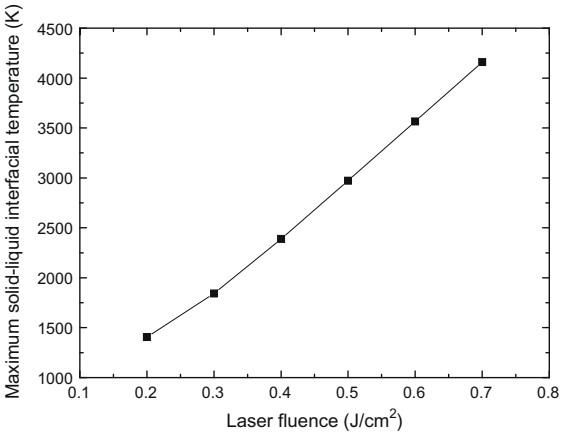

(a) Dependence of maximum solid-liquid interfacial temperature on laser fluence

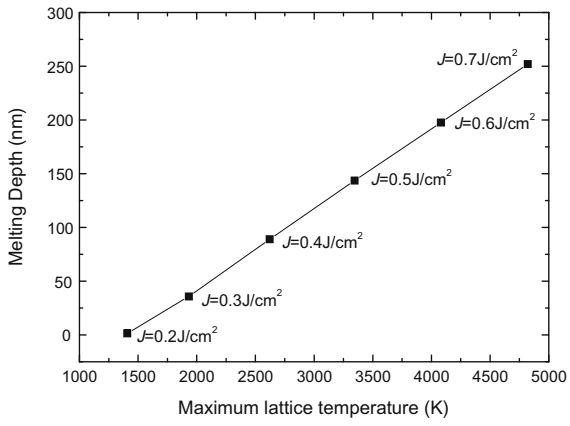

(b) Dependence of melting depth on maximum lattice temperature

Fig. 3. The relationship between laser fluence, maximum lattice temperature and melting depth with single pulse.

The liquid–vapor interfacial temperature is controlled by the energy balance and saturation pressure. Because of the backflow of evaporated vapor to the surface, the saturation pressure will be lifted, which leads to higher liquid–vapor interfacial temperature. Fig. 4(a) shows the dependence of maximum liquid–vapor interfacial temperature on laser fluence. Fig. 4(b) shows the relationship between the maximum ablation depth and maximum vaporization temperature. While higher pulse fluence leads to a deeper ablation, the ablation depth is much smaller than the melting depth. This shows that under $0.9T_c$, the ablation caused by evaporation is insignificant.

Figs. 3(b) and 4(b) will serve as the bases of the comparison between multiple pulses and single pulse. If the resultant point of a multiple pulses irradiation is located in the upper part of Fig. 3(b), it means with the same maximum temperature, multiple pulses will achieve deeper melting, and vice-versa. Similarly, a point of multiple pulses located in the upper part of Fig. 4(b) means with the same maximum temperature, multiple pulses will obtain deeper ablation depth. In other words, it means that multiple pulses can achieve the same ablation depth with lower temperature, which is desirable in laser-material processing.

4.2. Two pulses

Two consecutive pulses with same fluence and a separation time of Δt are studied first. A typical lattice temperature evolution

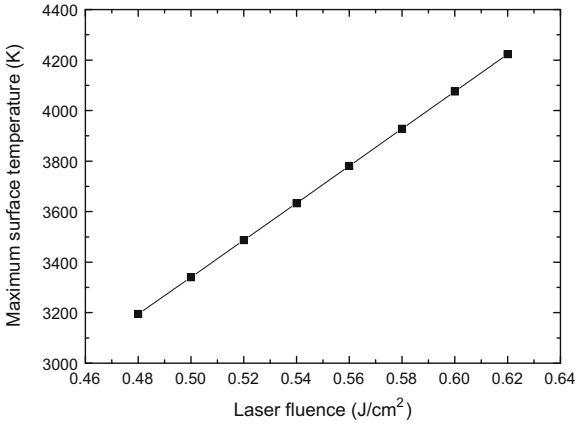

(a) Dependence of maximum surface temperature on laser fluence

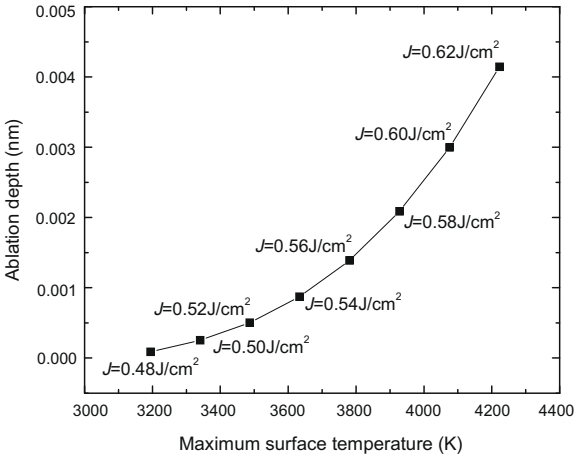

(b) Dependence of ablation depth on maximum temperature with single pulse

Fig. 4. The relationship between laser fluence, maximum surface temperature and ablation depth with single pulse.

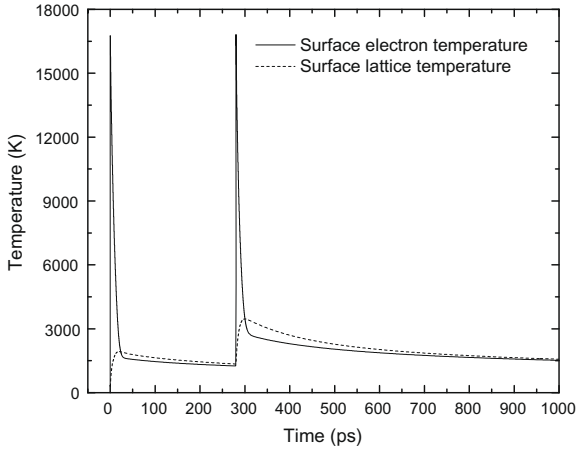

(a) Electron and lattice temperature

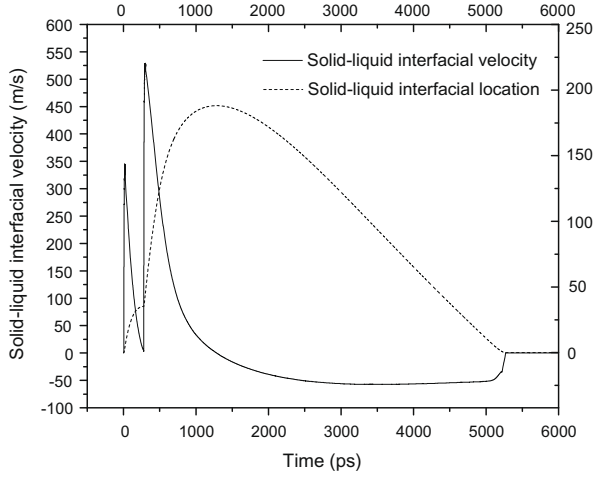

(b) Solid-liquid interfacial velocity and location

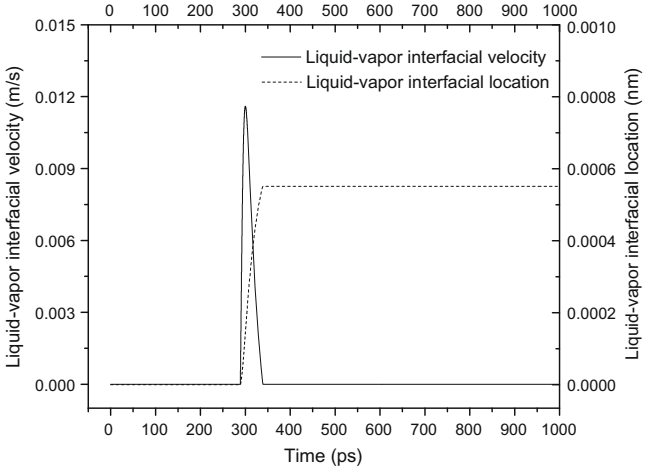

(c) Liquid-vapor interfacial velocity and location

Fig. 5. Irradiation by two consecutive 0.3 J/cm^2 laser pulses with a separation time of 280 ps.

with a separation time of 280 ps and single pulse fluence of 0.3 J/cm^2 is shown in Fig. 5. In Fig. 5(a), each pulse arouses a peak in electron and lattice temperature. The second peak of lattice temperature is much higher, because of the utilization of residual thermal energy deposited by the first pulse. The melting process is also intensified as indicated by Fig. 5(b). In Fig. 5(c), there is only one peak in liquid–vapor interfacial velocity, which is caused by the second pulse. This is because a single pulse of 0.3 J/cm^2 is lower than the threshold value for evaporation.

The irradiation processes caused by two 0.3 J/cm^2, 100 fs laser pulses with a separation time ranged from 10 ps to 6000 ps are then simulated. The dependence of maximum melting depth on maximum lattice temperature with different separation time is shown in Fig. 6(a). The arrows indicate the directions toward which the separation time Δt increases. The solid line in Fig. 6(a) is the result of single pulse, as shown in Fig. 3(b). All the results of two pulses are located in the upper side of the solid line, which means that with the same peak temperature, the melting depth of two pulses will always be deeper than that of a single pulse. Furthermore, it can be seen that when the separation time increases from 10 ps, the maximum temperature will decrease without an obvious drop of melting depth. The result points of two pulses deviate from the single pulse line gradually. When the aim of laser irradiation is to obtain deeper melting depth, this is a desirable trend because the same melting depth can be achieved with lower temperature, i.e., the residual thermal stress will be lower. However, when the separation time is longer than 280 ps, the result points of two pulses approach to the single pulse line again, melting depth drops soon with the same temperature. When the separation time equals to 800 ps, the difference between two

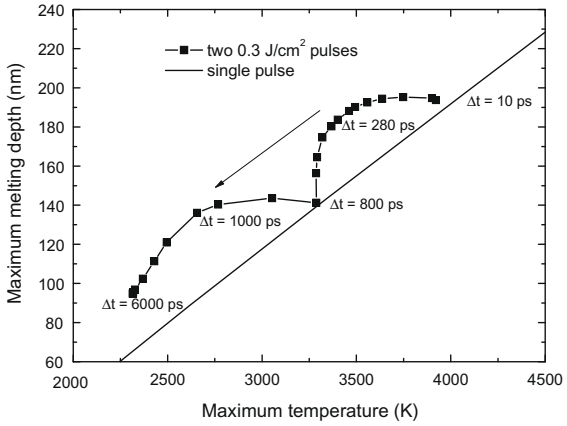

(a) Relationship between maximum temperature and melting depth

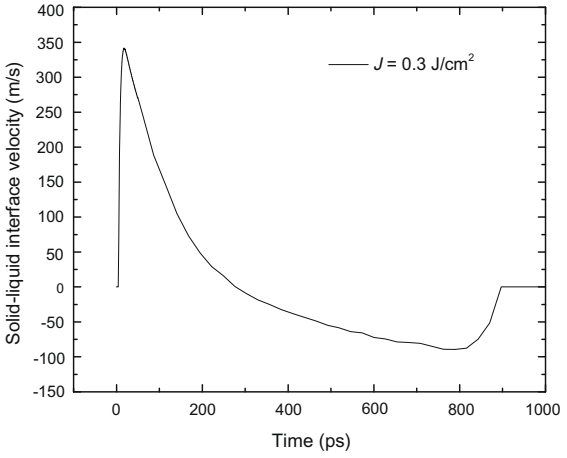

(b) Variation of solid-liquid interfacial velocity with time by a single 0.3J/cm^2 pulse

Fig. 6. Relationship between maximum temperature and melting depth by two consecutive 0.3 J/cm^2 laser pulses with separation time ranged from 10 ps and 6000 ps.

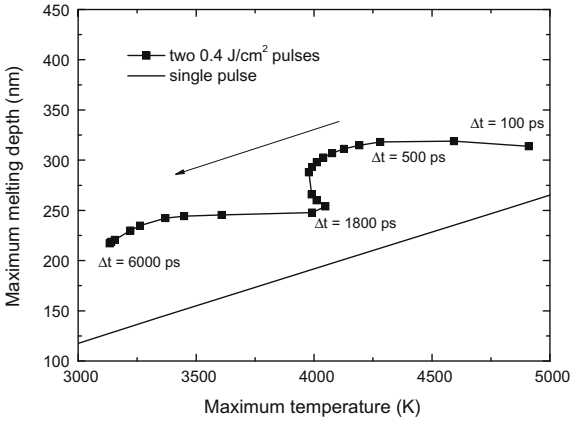

(a) Relationship between maximum temperature and melting depth

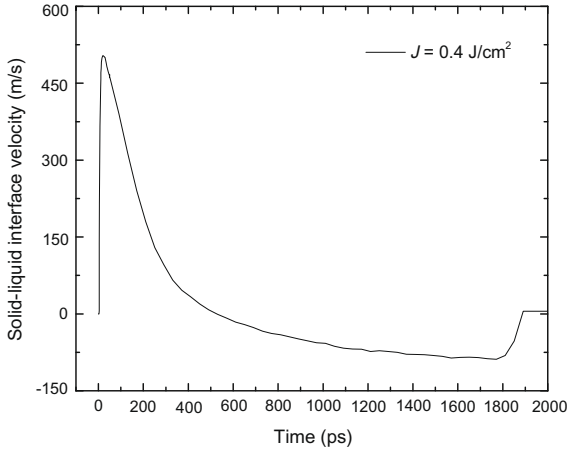

(b) Variation of solid-liquid interfacial velocity with time by a single 0.4J/cm^2 pulse

Fig. 7. Relationship between maximum temperature and melting depth by two consecutive 0.4 J/cm^2 laser pulses with separation time ranged from 100 ps and 6000 ps.

pulses and single pulse is very small. After that, with the increase of separation time, the results caused by two pulses will deviate from the solid line again. In comparison to Fig. 6(b), which is the variation of solid–liquid interface velocity, it can be found that 280 ps is just the time when the solid–liquid interfacial velocity turn from positive to negative, i.e., when the resolidification process starts; 800 ps is the time when the interfacial velocity achieves maximum negative value. Fig. 6 shows that if a deeper melting depth is the aim of laser metal interaction, the second pulse should be launched when the melting process caused by the first pulse reaches the maximum value. On the other hand, if the second pulse is launched when the resolidification process is about to stop, two pulses irradiation shows no advantage over the single pulse. To verify this, the irradiation process caused by two 0.4 J/cm^2 pulses is also simulated. The results are shown in Fig. 7, which shows the same findings as Fig. 6.

Fig. 8 shows the dependence of ablation depth caused by two 0.3 J/cm^2 pulses on the maximum surface temperature. In most cases, the ablation depth caused by two pulses is slightly deeper than a single pulse which would cause the same peak temperature. However, it should be noticed that when the separation time is around 20 ps, the points are located at the lower part of the solid line, which means smaller ablation depth. As shown in Fig. 8(b), the surface temperature variation with time caused by a single 0.3 J/cm^2 pulse, 20 ps is exactly the time that surface lattice temperature reaches peak. This means that if a deeper ablation depth is wanted, the second pulse should not be launched when the temperature caused by the first pulse reaches its peak value.

4.3. Multiple pulses

The cases of more than two pulses interaction with the gold film are also studied. To compare with a single pulse of 0.6 J/cm^2, six cases are considered: (a) 2 pulses at 0.3 J/cm^2 per pulse; (b) 3 pulses at 0.2 J/cm^2 per pulse; (c) 4 pulses at 0.15 J/cm^2 per pulse; (d) 5 pulses at 0.12 J/cm^2 per pulse; (e) 6 pulses at 0.1 J/cm^2 per pulse; (f) 10 pulses at 0.06 J/cm^2 per pulse. The separation time ranged from 1 ps to 15 ps.

Figs. 9 and 10 show the dependence of maximum temperature and melting depth on the number of pulses and separation time. It can be seen that with more pulses, the temperature and melting depth will decrease. The increase of separation time also leads to lower temperature and melting depth. If the relationship between maximum temperature and melting depth caused by multiple pulses is plotted and compared with that of a single pulse, Fig. 11 can be obtained. It is clear that all the points are located

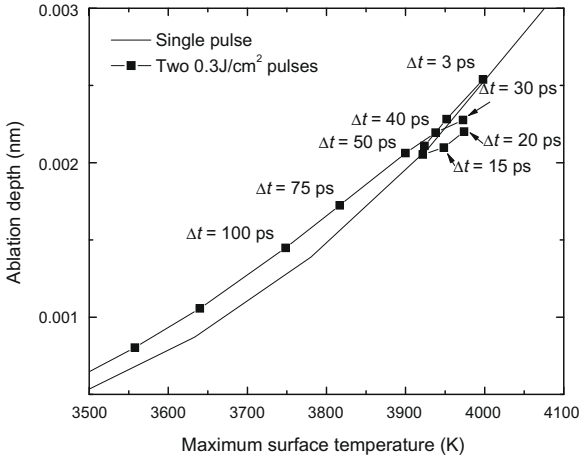

(a) Relationship between maximum temperature and ablation depth

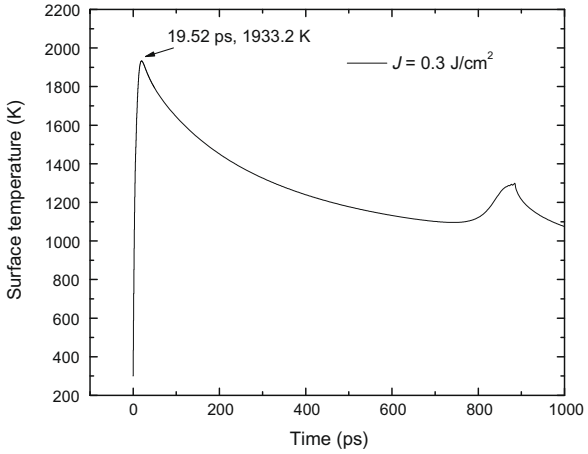

(b) Variation of surface temperature with time by a single 0.3J/cm^2 pulse

Fig. 8. Relationship between maximum temperature and ablation depth by two consecutive 0.3 J/cm^2 laser pulses with separation time ranged from 3 ps and 200 ps.

on the upper side of the single pulse line, which means deeper melting depth will be achieved with the same lattice temperature. And this difference will be larger with higher number of pulses and

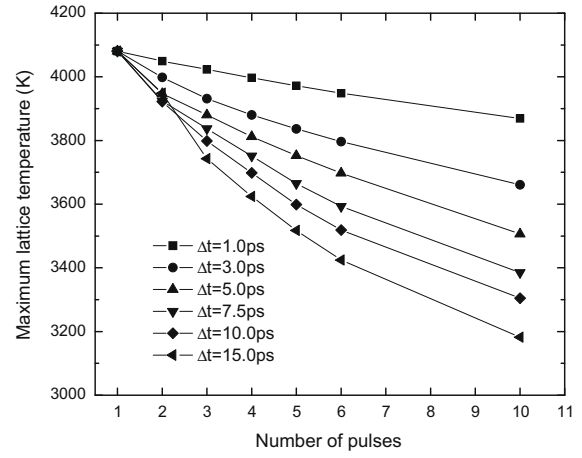

Fig. 9. Dependence of maximum temperature on pulses number and separation time.

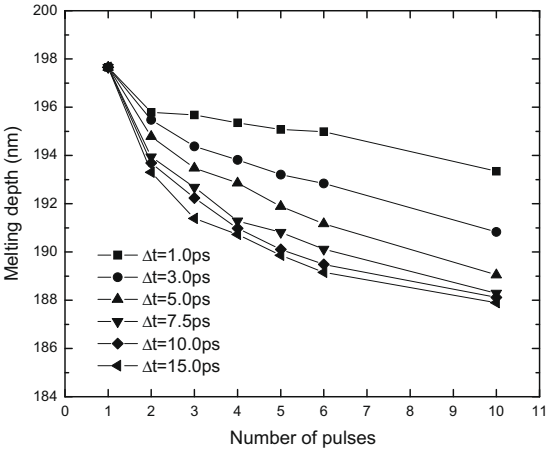

Fig. 10. Dependence of melting depth on pulses number and separation time.

longer separation time. In comparison to a single 0.6 J/cm^2 pulse irradiation, the maximum lattice temperature caused by 10 consecutive pulses with a separation time of 15 ps can reduce 22.01%, while the melting depth only decreases 4.93%. This means in practical application, if deeper melting is wanted, multiple pulses is preferable than the single pulse, because it will lead to lower temperature and consequently smaller residual stress and distortion.

Similarly, Figs. 12 and 13 show that larger pulse number and longer separation time will lead to lower surface temperature and smaller ablation. Fig. 14 shows the comparison between multiple pulses and single pulse. The points of multiple pulses are located just upon the solid line, which means that if the maximum temperature is controlled to be the same for multiple pulses and single pulse, using multiple pulses will not lead to much difference in ablation depth in comparison with a single pulse.

5. Conclusion

Rapid phase change processes including melting, vaporization and resolidification in a gold thin film irradiated by multiple laser pulses is investigated in this paper. A two-temperature model in conjunction with interfacial track method was employed to describe the temperature variation, solid–liquid and liquid–vapor interface evolution. The relationship between peak lattice temper-

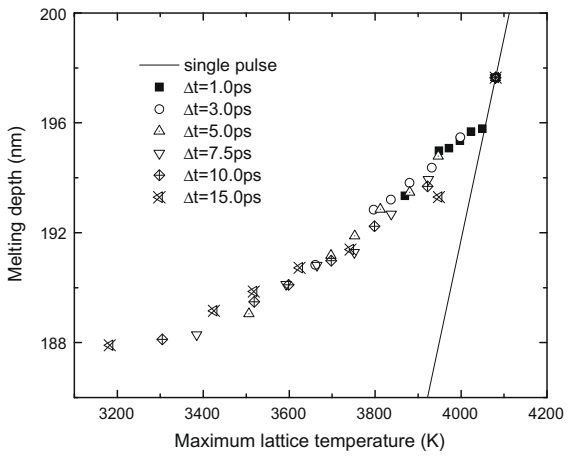

Fig. 11. Comparison of melting depth between multiple pulses irradiation and single pulse irradiation.

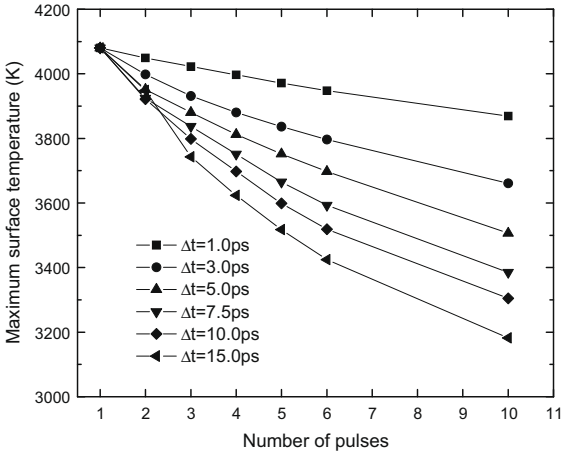

Fig. 12. Dependence of surface temperature on pulses number and separation time.

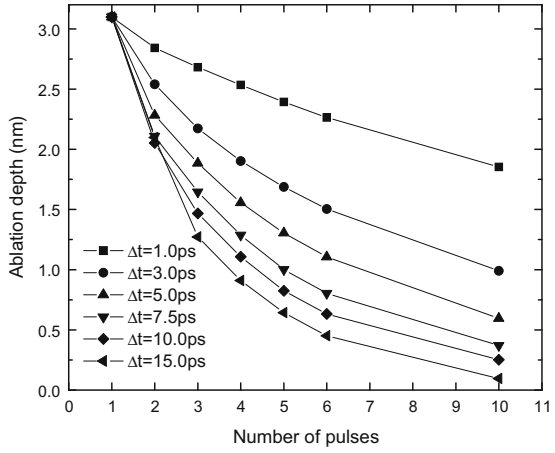

Fig. 13. Dependence of ablation depth on pulses number and separation time.

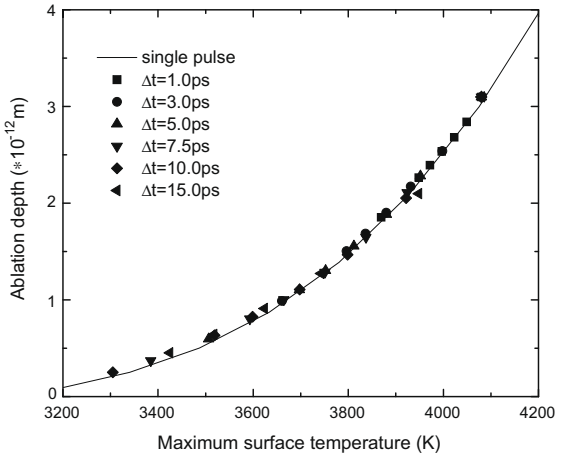

Fig. 14. Comparison of ablation depth between multiple pulses irradiation and single pulse irradiation.

ature and melting depth, ablation depth are analyzed and compared with that of the single pulse irradiation.

It is found that for two pulses irradiation, if deeper melting depth is desirable, the second pulse should be launched when the melting depth caused by first pulse reaches the peak. In comparison to single pulse irradiation with the same lattice temperature, this leads to a greater melting depth. If the second pulse is launched at the time when the resolidification process is about to end, two pulses irradiation shows no difference to a single pulse process. For ablation caused by evaporation, if the second pulse is launched when the surface temperature reaches the peak, ablation depth will be smaller than a single pulse.

For laser irradiation with more than two consecutive pulses, if the total laser fluence remains a constant, higher pulse number and longer separation times between pulses lead to smaller melting depth, but in comparison with a single pulse that causes the same lattice temperature, the melting depth is much deeper. At the same time, multiple pulses irradiation shows no advantage in ablation over single pulse with the same peak temperature.

Acknowledgement

Support for this work by the U.S. National Science Foundation under Grant No. CBET-0730143 is gratefully acknowledged.

References

[1] D.S. Ivanov, L.V. Zhigilei, Kinetic limit of heterogeneous melting in metals, Phys. Rev. Lett. 98 (19) (2007) 1957011–1957014.
[2] L.V. Zhigilei, D.S. Ivanov, E. Leveugle, B. Sadigh, E.M. Bringa, Computer modeling of laser melting and spallation of metal targets, in: C.R. Phipps (Ed.), Proceedings of SPIE, vol. 5448, SPIE, 2004, pp. 505–519.
[3] M. Agarwala, D. Bourell, J. Beaman, H. Marcus, J. Barlow, Direct selective laser sintering of metals, Rapid Prototyping J. 1 (1) (1995) 26–36.
[4] R.K. Ganesh, A. Faghri, Y. Hahn, A generalized thermal modeling for laser drilling processes: I. Mathematical modeling and numerical methodology, Int. J. Heat Mass Transfer 40 (14) (1997) 3351–3360.
[5] M. Shiomi, A. Yoshidome, F. Abe, K. Osakada, Finite element analysis of melting and solidifying processes in laser rapid prototyping of metallic powders, Int. J. Mach. Tools Manufact. 39 (2) (1999) 237–252.
[6] T. Zacharia, S.A. David, J.M. Vitek, T. Debroy, Heat transfer during Nd:Yag pulsed laser welding and its effect on solidification structure of austenitic stainless steels, Metall. Trans. A 20 (5) (1989) 957–967.
[7] Y. Zhang, A. Faghri, C.W. Buckley, T.L. Bergman, Three-dimensional sintering of two-component metal powders with stationary and moving laser beams, J. Heat Transfer 122 (1) (2000) 150–158.
[8] S.I. Anisimov, B.L. Kapeliovich, T.L. Perel'man, Electron emission from metal surfaces exposed to ultra-short laser pulses, Sov. Phys. JETP 39 (2) (1974) 375–377.
[9] T.Q. Qiu, C.L. Tien, Heat transfer mechanisms during short-pulse laser heating of metals, J. Heat Transfer – ASME 115 (4) (1993) 835–841.
[10] D.Y. Tzou, Macro- to Microscale Heat Transfer, Taylor & Francis, Washington, DC, 1997.
[11] D.Y. Tzou, Computational techniques for microscale heat transfer, in: W.J. Minkowycz, E.M. Sparrow, J.Y. Murthy, W.J. Minkowycz, E.M. Sparrow, J.Y. Murthy (Eds.), Handbook of Numerical Heat Transfer, second ed., Wiley, Hoboken, NJ, 2006.
[12] L. Jiang, H.L. Tsai, Improved two-temperature model and its application in ultrashort laser heating of metal films, J. Heat Transfer 127 (10) (2005) 1167–1173.
[13] J.K. Chen, D.Y. Tzou, J.E. Beraun, A semiclassical two-temperature model for ultrafast laser heating, Int. J. Heat Mass Transfer 49 (1–2) (2006) 307–316.
[14] J. Huang, Y. Zhang, J.K. Chen, Ultrafast solid–liquid–vapor phase change of a gold film induced by pico- to femtosecond lasers, unpublished.
[15] I.H. Chowdhury, X. Xu, A.M. Weiner, Ultrafast pulse train micromachining, in: J. Neev, A. Ostendorf, C.B. Schaffer (Eds.), Proceedings of SPIE, vol. 4978, 2003, pp. 138–146.
[16] J.K. Chen, J.E. Beraun, Superheating and material ablation of metals by multiple ultrashort laser pulses, J. Directed Energy (1) (2004) 93–109.
[17] L. Jiang, H.L. Tsai, Modeling of ultrashort laser pulse-train processing of metal thin films, Int. J. Heat Mass Transfer 50 (17–18) (2007) 3461–3470.
[18] S.I. Anisimov, B. Rethfeld, Theory of ultrashort laser pulse interaction with a metal, in: Proceedings of SPIE, vol. 3093, 1997, pp. 192–203.
[19] J.K. Chen, W.P. Latham, J.E. Beraun, The role of electron–phonon coupling in ultrafast laser heating, J. Laser Appl. 17 (1) (2005) 63–68.
[20] L.S. Kuo, T.Q. Qiu, Microscale energy transfer during picosecond laser melting of metal films, in: ASME National Heat Transfer Conference, 1996, pp. 149–157.
[21] P.G. Klemens, R.K. Williams, Thermal conductivity of metals and alloys, Int. Met. Rev. 31 (5) (1986) 197–215.
[22] A. Faghri, Y. Zhang, Transport Phenomena in Multiphase Systems, Elsevier Academic Press, Burlington, MA, 2006.
[23] X. Xu, G. Chen, K.H. Song, Experimental and numerical investigation of heat transfer and phase change phenomena during excimer laser interaction with nickel, Int. J. Heat Mass Transfer 42 (8) (1999) 1371–1382.

[24] N. Birks, G.H. Meier, F.S. Pettit, Introduction to the High-Temperature Oxidation of Metals, second ed., Cambridge University Press, Cambridge, 2006.
[25] I. Akhatov, O. Lindau, A. Topolnikov, R. Mettin, N. Vakhitova, W. Lauterborn, Collapse and rebound of a laser-induced cavitation bubble, Phys. Fluids 13 (10) (2001) 2805–2819.
[26] Y. Zhang, J.K. Chen, An interfacial tracking method for ultrashort pulse laser melting and resolidification of a thin metal film, J. Heat Transfer 130 (6) (2008) 0624011–06240110.
[27] I. Barin, Thermochemical Data of Pure Substance. Part I, VCH, New York, 1993.